Acta Pharmaceutica Sinica B 2019;9(2):397–409

Chinese Pharmaceutical Association
Institute of Materia Medica, Chinese Academy of Medical Sciences

Acta Pharmaceutica Sinica B

www.elsevier.com/locate/apsb
www.sciencedirect.com

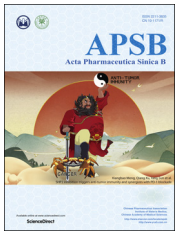

ORIGINAL ARTICLE

Transformative hyaluronic acid-based active targeting supramolecular nanoplatform improves long circulation and enhances cellular uptake in cancer therapy

Lu Zhong[a], Lu Xu[a], Yanying Liu[a], Qingsong Li[a], Dongyang Zhao[a], Zhenbao Li[a], Huicong Zhang[a], Haotian Zhang[b], Qiming Kan[b], Yongjun Wang[a], Jin Sun[a,*], Zhonggui He[a,*]

[a]*Department of Pharmaceutics, Wuya College of Innovation, Shenyang Pharmaceutical University, Shenyang 110016, China*
[b]*Department of Pharmacy, Shenyang Pharmaceutical University, Shenyang 110016, China*

Received 23 July 2018; received in revised form 2 October 2018; accepted 2 November 2018

KEY WORDS

Hyaluronic acid;
Benzoic imine linkage;
Active-targeting;
Cancer therapy;

Abstract Hyaluronic acid (HA) is a natural ligand of tumor-targeted drug delivery systems (DDS) due to the relevant CD44 receptor overexpressed on tumor cell membranes. However, other HA receptors (HARE and LYVE-1) are also overexpressing in the reticuloendothelial system (RES). Therefore, polyethylene glycol (PEG) modification of HA-based DDS is necessary to reduce RES capture. Unfortunately, pegylation remarkably inhibits tumor cellular uptake and endosomal escapement,

Abbreviations: ADA, 1-adamantane carboxylic acid; AD-B-PEG, the pH-responsive adamantane-PEG conjugate; AD-O-PEG, the non-pH sensitive adamantane-PEG conjugate; AUC, area under the plasma concentration–time curve; CLSM, confocal laser scanning microscope; DAPI, 2-(4-amidinophenyl)-6-indolecarbamidine dihydrochloride; DCC, *N,N′*-dicyclohexylcarbodiimide; DCM, dichloromethane; DDS, drug delivery systems; DiR, 1,1′-dioctadecyltetramethyl indotricarbocyanine iodide; DL, drug-loading content; DLS, dynamic light scattering; DMAP, 4-dimethylaminopyrideine; DMEM, Dulbecco's modified Eagle's medium; Dox · HCl, doxorubicin hydrochloride; Dox/HCVBP, Dox-loaded hyaluronic acid-based transformable supramolecular nanoplatform; Dox/HCVOP, Dox-loaded hyaluronic acid-based untransformable supramolecular nanoplatform; EDC, 1-ethyl-3-(3-dimethylaminopropl) carbodiimide; EE, encapsulation efficiency; FBS, fetal bovine serum; HA, hyaluronic acid; HA-CD, hydroxypropyl-*β*-cyclodextrin grafted hyaluronic acid polymer; HCBP, hydroxypropyl-*β*-cyclodextrin grafted hyaluronic acid polymer and pH-responsive adamantane-PEG conjugate inclusion complex; HCPs, hydroxypropyl-*β*-cyclodextrin grafted hyaluronic acid polymer and adamantane-PEG conjugate inclusion complexes; HEPES, 4-(2-hydroxyethyl)-1-piperazineethanesul-fonic acid; H&E, hematoxylin and eosin; HOBT, 1-hydroxybenzotriazole; HPCD, hydroxypropyl-*β*-cyclodextrin; MW, molecular weight; NPs, nanoparticles; PCC, Pearson's correlation coefficient; PDI, polydispersity index; pH_e, the extracellular pH; RES, reticuloendothelial system; RPMI-1640, Roswell Park Memorial Institute-1640; THF, tetrahydrofuran; TUNEL, terminal deoxynucleotidyl transferased dUTP nick end labeling; VES, vitamin E succinate

*Corresponding authors.
E-mail addresses: sunjin@syphu.edu.cn (Jin Sun), hezhgui_student@aliyun.com (Zhonggui He).

Peer review under responsibility of Institute of Materia Medica, Chinese Academy of Medical Sciences and Chinese Pharmaceutical Association.

https://doi.org/10.1016/j.apsb.2018.11.006

Natural ligand;
Supramolecular nanoplatform;
Transformative nanoparticles;
PEG dilemma

significantly compromising the *in vivo* antitumor efficacy. Herein, we developed a Dox-loaded HA-based transformable supramolecular nanoplatform (Dox/HCVBP) to overcome this dilemma. Dox/HCVBP contains a tumor extracellular acidity-sensitive detachable PEG shell achieved by a benzoic imine linkage. The *in vitro* and *in vivo* investigations further demonstrated that Dox/HCVBP could be in a "stealth" state at blood stream for a long circulation time due to the buried HA ligands and the minimized nonspecific interaction by PEG shell. However, it could transform into a "recognition" state under the tumor acidic microenvironment for efficient tumor cellular uptake due to the direct exposure of active targeting ligand HA following PEG shell detachment. Such a transformative concept provides a promising strategy to resolve the dilemma of natural ligand-based DDS with conflicting two processes of tumor cellular uptake and *in vivo* nonspecific biodistribution.

1. Introduction

Hyaluronic acid (HA) is an endogenous polysaccharide composed of a simple repeating disaccharide of D-glucuronic acid and *N*-acetyl-D-glucosamine linked by $\beta(1\rightarrow3)$ linkages. HA possesses superior characteristics as a nanocarrier and an active targeting moiety of nanoparticles (NPs) for cancer therapy since it is a ligand of CD44 receptor overexpressed on numerous tumor cell membranes[1–3]. Unfortunately, HA is also a ligand of another HA receptor (such as HARE and LYVE-1) usually expressed in the reticuloendothelial system (RES), which results in unexpected off-target biodistribution of HA-based NPs in RES and rapid clearance of NPs from blood[4,5]. Despite relatively high expression in tumors, similar nonspecific distribution pattern also could be found for folate receptor, transferrin receptor, etc.[6–9] Accordingly, active targeting NPs based on these endogenous natural ligands usually suffer from nonspecific distribution in the body due to a far larger mass of normal tissues than tumor tissue in spite of good biocompatibility[10–15]. Those works have demonstrated that PEGylation could effectively reduce RES capture, prolong the circulation time and enhance the accumulation of tumor site after intravenous administration. Unfortunately, such a successful strategy compromises tumor cellular uptake and results in poor endosomal escapement and low targeting efficacy, that is "polyethylene glycol (PEG) dilemma"[16,17].

In recent years, many smart stimuli-responsive NPs have achieved on-demand delivery, including external or tumor internal stimulus (temperature, magnetic force, light, redox, pH, enzyme, and hypoxia)[11,18–22]. In general, the physicochemical properties of stimuli-responsive NPs (such as size, surface charge, and surface targeting ligand) would change under the specific stimulus to modulate their interactions with biological systems[23–28]. Taking advantage of tumor microenvironments is a promising approach to address the "PEG dilemma", and significant efforts have been made. The PEG was modified with chemical or enzymatic sensitive bonds (such as the disulfide bond, Schiff base bond, and benzoic imine bond) to prepare the detachable pegylated layer[11,29–38]. These strategies could efficiently improve the cellular uptake or facilitate the endosomal escapement for enhancing intracellular drug delivery. Detachable pegylation layer could be more meaningful for natural ligand-mediated targeting drug delivery systems (DDS), but there are little relevant reports on it.

It is known that the extracellular pH (pH_e 6.5) of tumor microenvironment is lower than normal tissues (pH_e 7.4) due to the high rate of glycolysis in cancer cells[39–41]. Some pH-responsive linkages provide a facile approach to achieve pH-sensitive NPs for improved antitumor efficacy, such as histidine, β-amino ester, ortho ester, and benzoic imine[27,42–45]. The benzoic imine linkage attracted much attention due to its rapid cleavage under tumor pH_e condition but good stability at the physiological pH.[46,47] Wei et al.[44,48–51] have successfully used it to elicit the charge reversion or ligand exposure of NPs at tumor pH_e for enhanced intercellular delivery of cargos.

Herein, we explored a transformable tumor targeting Dox-loaded HA supramolecular nanoassembly for overcoming the "PEG dilemma" with the aid of benzoic imine linker, termed as Dox/HCVBP. Specifically, the hydroxypropyl-β-cyclodextrin (HPCD)-grafting HA polymer (HA-CD) and the pH-responsive adamantane-PEG conjugate (AD-B-PEG) with the benzoic imine linkage were synthesized. The non-pH sensitive adamantane-PEG conjugate (AD-O-PEG) was also synthesized as a negative control. Then Dox/HCVBP NPs were prepared by the host-guest inclusion interaction of cyclodextrin and adamantane with the help of hydrophobic molecular vitamin E succinate (VES) (Fig. 1). The VES served as a nanobridge to connect HPCD grafted HA and Dox and could significantly improve drug encapsulation efficiency, NPs stability and sustain drug release[10]. After Dox/HCVBP was intravenously administrated, it would keep the "stealth" state in the blood stream due to the buried of HA and the reduced interaction with biosystem by PEG shell. The "stealth" PEG layer would be removed to expose the buried HA ligands at tumor microenvironment and then the NPs could transform into the "recognition" state for improving cellular uptake *via* HA-mediated endocytosis. After endocytosis, the increased acidity in the endo/lysosomes would further accelerate the release of Dox for an enhanced antitumor effect (Fig. 1). We systematically investigated the physiochemical and pharmaceutical properties of the transformative NPs and evaluated the effect on its overall antitumor effect. Such pH-sensitive modification of PEG would effectively overcome "PEG dilemma" for improving the long circulation time and enhancing intracellular drug delivery.

2. Materials and methods

2.1. Materials

HA-CD (HA molecular weight, MW = 63 kDa) was previously obtained by carboxyl of HA and hydroxy of HPCD reaction with the catalyzation of 1-ethyl-3-(3-dimethylaminopropl) carbodiimide (EDC) and 1-hydroxybenzotriazole (HOBT). Vitamin E succinate

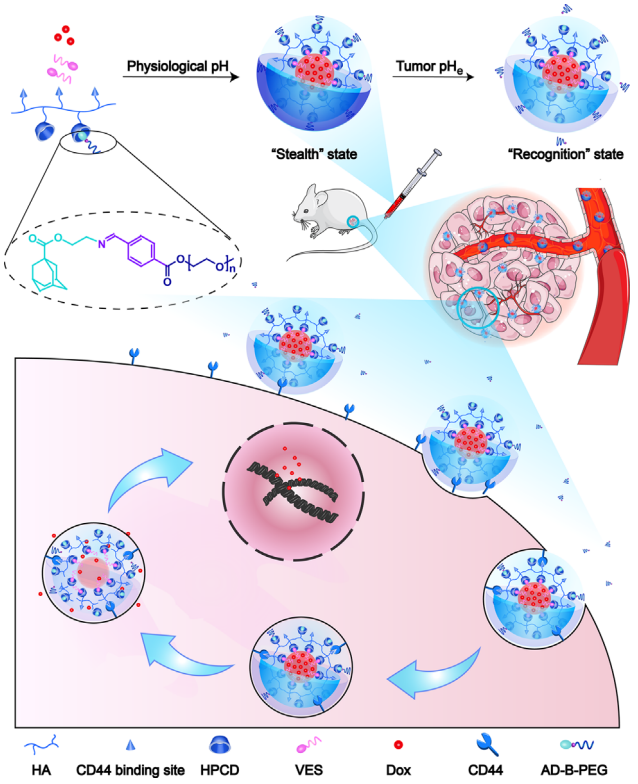

Figure 1 Schematic illustration of transformable Dox/HCVBP nanoparticle structure and targeting tumor delivery. Dox/HCVBP could be in a "stealth" state at blood stream to prolong circulation time due to the PEG shell and transform into a "recognition" state under the tumor acidic microenvironment following PEG shell detachment to enhance tumor cellular uptake. And the PEG shell could be detached more completely in endo/lysosomes, which is advantageous to the endosomal escape of NPs for enhancing antitumor efficacy.

(VES), mPEG 5000 and 1-adamantane carboxylic acid (ADA) were purchased from Sigma–Aldrich (St. Louis, MO, USA). *N*,*N*′-dicyclohexylcarbodiimide (DCC) and 4-dimethylaminopyrideine (DMAP) were obtained from Pukang pharm Co., Ltd. (Quzhou, China). Fetal bovine serum (FBS), 4-(2-hydroxyethyl)-1-piperazineethanesulfonic acid (HEPES), the near infrared lipophilic carbocyanine dye 1,1′-dioctadecyltetramethyl indotricarbocyanine iodide (DiR) and 2-(4-amidinophenyl)-6-indolecarbamidine dihydrochloride (DAPI) were provided by Dalian meilun biotechnology Co., Ltd. (Dalian, China). Doxorubicin hydrochloride (Dox · HCl) was purchased from Huafeng United Technology Co., Ltd. (Beijing, China), and was deprotonated with twice the molar amount of triethylamine as a hydrochloride scavenging agent to obtain the hydrophobic Dox for use. Other organic solvents or reagents were analytic grade and used as received.

2.2. *Synthesis and characterization of the non-pH sensitive adamantane-PEG conjugate (AD-O-PEG)*

AD-O-PEG was synthesized as previously described with a little modification[10,52,53]. Briefly, the catalysts DCC (0.36 g, 1.8 mmol) and DMAP (0.1 g, 0.8 mmol) were added to a solution of ADA (0.16 g, 0.9 mmol) in 10 mL water-free dichloromethane (DCM). After stirred for 2 h in an ice-bath, the mPEG 5000 (1.5 g, 0.3 mmol) dissolved in 5 mL anhydrous DCM was dropwise added. The reaction mixture was stirred at 30 °C under the atmosphere of N_2 for 48 h. Then the solution was cooled at –20 °C overnight and filtered to remove impurities. The filtrate was concentrated, precipitated by absolute ethyl ether for three times, recrystallized with isopropanol for purification and vacuum-dried for 4 h to gain the final product. ^{1}H NMR (600 MHz, $CDCl_3$, TMS, δ): 3.38 (s, -O-CH_3), 3.82 (t, -CH_2-CH_2OC=O), 4.20 (t, -CH_2-OC=O), 1.71–2.13 (m, -CH_2- and -CH-of adamantyl moiety), 3.54–3.72 (m, methylene of PEG).

2.3. *Synthesis of 4-carboxybenzaldehyde modified mPEG (compound **1**)*

There were three steps to synthesize the AD-B-PEG[47,54]. Firstly, 4-carboxybenzaldehyde (1.8 g, 12 mmol) and DMAP (0.04 g, 0.3 mmol) were put into a flask, and 50 mL anhydrous tetrahydrofuran (THF) was added under the atmosphere of argon gas. DCC (1.24 g, 6 mmol) dissolved in 10 mL anhydrous THF was dropped into the above solution slowly by a syringe within 30 min. Then mPEG 5000 (3 g, 0.6 mmol) was added, and the liquid was stirred at 30 °C for 24 h. The mixture was filtered to remove insoluble by-product before the solvent was evaporated by a rotary (rotary vacuum evaporation, Yarong, Shanghai). The rough product was dissolved in absolute methanol and precipitated with absolute ethyl ether. The precipitation was recrystallized by isopropanol three times to purify the product. We gained compound **1** after drying for 4 h under vacuum.

2.4. *Synthesis of ethanolamine modified adamantane-1-carboxylic acid (compound **2**)*

Ethanolamine (1.83 g, 30 mmol), Al_2O_3 (8.15 g, 80 mmol) and methane sulfonic acid (26 mL, 400 mmol) were added into a 100 mL round-bottom flask and blended well under the atmosphere of argon gas. Then adamantane-1-carboxylic acid (3.6 g, 20 mmol) was added. After refluxed for 6 h at 75 °C, the mixture was poured into 1000 mL 5% sodium carbonate solution until there were no bubbles. The solution was extracted with ethyl acetate. Obtained organic phase was dried with calcium chloride anhydrous, filtered and evaporated by a rotary to get the compound **2**.

2.5. *Synthesis and characterization of the pH sensitive adamantane-PEG conjugate (AD-B-PEG)*

Compound **1** (2 g, 0.4 mmol) and compound **2** (1.8 g, 8 mmol) were put in a 50 mL flask, and 50 mL anhydrous THF and trimethyl orthoformate (20 mL, 188 mmol) were added. Then the mixture was stirred under reflux condition for 24 h at 45 °C. After removing the solvent by rotary evaporation, the solid was recrystallized with isopropanol for three times, washed with ethyl ether at last time and vacuum-dried for 4 h to gain compound **3**, the final product AD-B-PEG. ^{1}H NMR (600 MHz, $CDCl_3$, TMS, δ): 3.38 (s, -O-CH_3), 4.38 (t, N-CH_2-$\underline{CH_2}$-), 4.49 (t, -CH_2OC=O), 7.80 (d, -CH- of benzene ring), 8.11 (d, -CH- of benzene ring), 8.33 (s, CH=N), 1.66–1.96 (m, -CH_2- and -CH-of adamantyl moiety), 3.64–3.88 (m, methylene of PEG, overlapped with N-CH_2-).

2.6. *Preparation of HA-CD/AD-PEG inclusion complex*

HA-CD/AD-PEG inclusion complex (HCPs) was obtained by dissolving HA-CD and AD-O-PEG/AD-B-PEG in pH 7.4 HEPES buffer and stirring at room temperature for 24 h. Then the mixture

was lyophilized to gain white powder for use. HCPs with 5% molar ratio of PEG and HA was prepared for constructing nanoparticles.

2.7. The pH-dependent hydrolysis of the polymer

For AD-B-PEG, the pH-dependent hydrolysis of the benzoic imine was assayed by the fluorescamine method[55]. Briefly, AD-B-PEG was dissolved in different buffers (pH 7.4, 6.5, and 5.0) with a final concentration of 1 mg/mL respectively, then incubated for the specified time at 37 °C under oscillation. Then 20 μL of each sample was added into 200 μL fluorescamine acetone solution (50 μg/mL) in a black 96-well plate. After incubation at room temperature for 10 min, the fluorescence intensity was measured at the excitation wavelength of 382 nm and the emission wavelength of 474 nm using a BioRad microplate reader (Model 500, USA). All the processes should be away from light. The fluorescence intensity of the sample incubated in 20 nmol/L acetic acid for 48 h and blank buffer solution were treated as the positive control (100% exposed of amine) and negative control (0%), respectively.

For HA-CD/AD-B-PEG inclusion complex (HCBP), the pH-dependent hydrolysis was characterized by ^{1}H nuclear magnetic resonance spectrometer (^{1}H NMR, Bruker-600 MHz, Switzerland)[54]. HCBP with 10% molar ratio of PEG and HA was prepared, and the structure analysis was performed on HCBP solutions in D_2O at a required pH adjusted by DCl or NaOD.

2.8. Preparation and characterization of Dox-loaded PEG-modified HA-CD nanoparticles

Dox-loaded PEG-modified HA-CD nanoparticles (Dox/HCVPs) were prepared by the emulsion solvent evaporation method. Briefly, 1 mL DCM organic solution containing 2 mg VES and 0.5 mg Dox was mixed completely with 4 mL water phase (pH 7.4 HEPES buffer) consisting of 10 mg HCPs. Then the mixture was subjected to sonication using a probe-type sonifier at 100 W for 10 min (turn on for 2 s with a 3 s interval) in an ice bath and the organic solvent was removed by rotary evaporation technology. After another 6 min ultrasound in the same condition, the final micellar solution was centrifuged at 10,000 × *g* for 10 min and filtered through 0.45 μm filter. The preparation of DiR-loaded micelles was similar to the steps listed above with the exception that Dox was replaced by DiR.

The average size, size distribution polydispersity index (PDI) and zeta potential of nanoparticles were measured by dynamic light scattering (DLS) using Malvern Zetasizer (Nano ZS, Malvern, UK) at 25 °C and the measurements were repeated in triplicate. The colloidal stability of nanoparticle stored at 4 °C was explored by investigating the average size at time intervals by DLS. The morphology of nanoparticles was visualized by JEM-2100 transmission electron microscope (TEM, JEOL, Japan). The negatively stained method was used on a carbon-coated copper grid with 2% phosphotungstic acid. To calculate the encapsulation efficiency (EE) and drug loading content (DL) of nanoparticles, the amount of Dox was measured by using ultraviolet-visible (UV–Vis) spectrophotometry at 485 nm. And the EE and DL were calculated using the Eqs. (1) and (2), respectively:

$$\mathrm{EE}\ (\%) = \left(\text{Amount of loaded Dox}/\text{Total amount of Dox}\right) \times 100 \quad (1)$$

$$\mathrm{DL}\ (\%) = \left(\text{Weight of loaded Dox}/\text{Weight of loaded Dox and carrier}\right) \times 100 \quad (2)$$

2.9. In vitro pH-responsive release behavior of Dox-loaded nanoparticles

The *in vitro* release behavior was carried out by dialysis method using dialysis membrane bag (MW cut-off 14 kDa) in different phosphate buffers (pH 7.4, 6.5 and 5.0 PBS). One milliliter of preparation was transferred into a dialysis bag and immersed in 30 mL above different mediums, then shaken in a water bath at 100 rpm at 37 °C. At predetermined intervals, 1 mL release medium was withdrawn and refilled another 1 mL fresh medium. The concentrations of Dox were determined by HPLC method after filtration through 0.22 μm filter membrane. And all experiments were conducted in triplicate.

2.10. Cell culture

All cells were cultured in an incubator at 37 °C with 5% CO_2 and 95% relative humidity and were subcultured with 0.25% trypsin–EDTA in PBS. Hela cells were maintained in Dulbecco's modified Eagle's medium (DMEM) supplemented with 10% FBS and 1% penicillin–streptomycin. H460 and 4T1 cells were maintained in Roswell Park Memorial Institute-1640 (RPMI-1640) medium containing 10% FBS and 1% penicillin–streptomycin.

2.11. CD44 receptor expression

The level of CD44 expression of various cells was investigated by immunofluorescence analysis. Generally, Hela, H460 and 4T1 cells were plated on glass coverslips in 24-well plate at a density of 1×10^5 cells/well for growing 24 h. After fixed with 4% paraformaldehyde, the cells were incubated with the anti-CD44 antibody (Abcam 119348, 1:200) overnight at 4 °C and with the secondary antibody Dlight-488 conjugated IgG for 30 min at 37 °C. The nuclei were stained by DAPI. Finally, the slides were mounted with antifade mounting medium (Beyotime, P0126) and observed with confocal laser scanning microscope (CLSM, Nikon C2SI, Japan). The CD44 expression of 4T1 bearing mice tumor tissue was also analyzed by CLSM. Tumor tissue was frozen in OCT embedding medium and 20 μm thickness frozen sections were prepared. After washed with PBS, the samples were treated with the similar procedure as above.

2.12. In vitro cytotoxicity of Dox/HCVPs

The cytotoxicity effect of Dox/HCVPs on Hela and H460 cells was evaluated by MTT assay. Briefly, the cells (5000 cells per well) in a logarithmic growth phase were seeded in 96 well plates and incubated for 24 h. Then they were treated with different concentrations of various formulations for 48 h. The solutions were aspirated, and then 100 μL fresh medium and 20 μL of MTT solution (5 mg/mL in PBS) were added. After incubation for 4 h at 37 °C, the contents were removed and 200 μL DMSO was added to dissolve the purple formazan products. The absorbances at 570 nm were read using a BioRad microplate reader (Model 500, USA). The median inhibitory concentration (IC_{50}) was determined with the software GraphPad Prism 5 (GraphPad Software, San Diego, USA). The Dox/HCVPs were pretreated under pH 6.5 condition for 30 min at 37 °C before use.

2.13. Cellular uptake of Dox/HCVPs

For flow cytometry, the cells were plated on a 6-well plate (0.5 million cells per well) and cultured for 24 h. Various preparations which diluted in serum-free media (the final concentration of 10 μg/mL of Dox) were added to the cells, with serum-free media-treated cells as the control. After 1 and 3 h of incubation at 37 °C, the medium was discarded, and the cells were washed three times with ice-cold PBS, detached by trypsin, harvested by centrifugation (500 g, 5 min) and washed with PBS three times again. At last, the cells were further resuspended in 0.3 mL of PBS for analysis based on the fluorescence of Dox by a flow cytometer (BD Biosciences, Oxford, UK).

2.14. Mechanism of Dox/HCVPs cellular uptake

On the one hand, the cellular uptake of Dox/HCVPs without and with pretreated under pH 7.4 and 6.5 conditions for 30 min at 37 °C on Hela cells was measured by flow cytometer. On the other side, their cellular uptake was investigated on Hela cells with or without pre-incubated with excessive free HA. Briefly, Hela cells were seeded in 6-well plate (0.5 million cells per well) and allowed to culture for 24 h. Free HA (MW 102 kDa, 5 mg/mL) was added to each well to pre-incubate for 1 h. Then the mediums were replaced with nanoparticles along with free HA (the same concentration as pre-incubation). After culturing for 3 h at 37 °C, the cells were washed with cold PBS, harvested and analyzed using flow cytometer.

2.15. Intracellular trafficking of Dox/HCVPs by CLSM

Hela cells were seeded onto glass coverslips in 24-well plate (0.1 million cells per well) and grown for 24 h. The cells were treated with Dox/HCVPs nanoparticles (pretreated under pH 6.5 condition for 30 min at 37 °C) for predetermined time periods. Then the cells were washed with cold PBS for three times and stained with LysoGreen (KeyGen Biotech, Jiangsu, China, KGMP006-2) for 30 min at 37 °C. After fixed with 4% paraformaldehyde and stained the cellular nuclei with DAPI, the slides were mounted with antifade mounting medium (Beyotime, P 0126) for visualizing with CLSM. To quantify the endosomal escape ratio of nanoparticles, the colocalization coefficient Pearson's correlation coefficient (PCC) was quantified using Image pro plus 6.0 software (Media Cybernetics, Rockville, USA). Results were presented as the mean of 10 individual cells.

2.16. Animals and tumor xenograft model

All animal experimental procedures were approved by the Institutional Animal Care and Use Committee of Shenyang pharmaceutical university (Shenyang, China) and were performed in compliance with the principles of care and use of laboratory animals. All animals were kept under specific pathogen-free (SPF) conditions and allowed free access to food and water. BALB/c mice (female, 20 g) were chosen to establish the 4T1 tumor xenograft model obtained *via* subcutaneous injections with 10^7 4T1 cells (suspended in 100 μL PBS) into the right hind leg.

2.17. In vivo pharmacokinetic and biodistribution of Dox/HCVPs

The male Sprague–Dawley (SD) rats weighing 200–220 g were randomly divided into three groups ($n=5$). Rats were administrated with a 5 mg/kg dose of Dox solution or Dox/HCVPs as a single injection through the tail vein, respectively. At scheduled time points, 300 μL of blood was drawn from the retro-orbital plexus of the rat eye and put into heparinized tubes. Supernatant plasma was obtained after centrifugation and stored at –80 °C for measuring. The concentration of Dox in the plasma was determined by UPLC–MS/MS, and the pharmacokinetic parameters including the area under the plasma concentration–time curve (AUC) and terminal half-life ($t_{1/2}$) were calculated using DAS 2.1.1 software (Chinese Pharmacokinetic Society, Beijing, China).

For imaging to study the biodistribution of nanoparticles, 4T1 tumor-bearing mice were administrated with free DiR, DiR-loaded HCVPs (2 mg/kg) *via* tail vein injection when tumor size reached 200–300 mm^3. Mice were sacrificed at pre-determined time points, and the major organs and tumors were dissected for *ex vivo* imaging using Caliper LifeSciences LIVIS® Lumina Series *iu* (PerkinElmer, MA, USA) with the parameters for DiR: excitation = 745 nm, emission = 800 nm.

2.18. In vivo antitumor efficacy of Dox/HCVPs

When the tumor volume reached around 200 mm^3, the 4T1 tumor-bearing mice were randomly divided into four groups ($n=5$) and treated with saline, Dox solution, Dox/HCVOP and Dox/HCVBP by injecting through tail vein with equivalent Dox dose (7 mg/kg, injection volume about 0.2 mL/10 g) three times at a 3-day interval, respectively. The tumor length (L) and width (W) were measured using digital caliper every 3 days, and the body weight of mice was recorded at the same time. Tumor volume (V, mm^3) was calculated based on Eq. (3):

$$V = W^2 \times L/2 \tag{3}$$

On day 15, all the mice were sacrificed, and tumors were harvested, weighed and photographed. The tumor burden was calculated with the Eq. (4):

$$\text{Tumor burden (\%)} = \text{Tumor weight}/\text{Body weight} \times 100 \tag{4}$$

Thereafter, the tumor tissues were fixed, embedded, sliced for hematoxylin and eosin (H&E) staining and terminal deoxynucleotidyl transferased dUTP nick end labeling (TUNEL) assay (KeyGen Biotech, KGA 7051). The TUNEL assay was conducted according to the manufacturer's instructions. The cell nuclei were stained with DAPI, and the samples were observed with CLSM.

2.19. Statistical analysis

All data were presented as mean ± SD (standard deviation). The data was calculated from a minimum of three independent trials. One-way analysis of variance (ANOVA) or Student's t-test was applied to evaluate significant differences among the treatment groups, and P value of 0.05 or less was considered to be statistically significant.

3. Results and discussion

3.1. Synthesis and characterization of conjugates

The HPCD grafted HA (HA-CD, grafted density is about 50%) was previously obtained by carboxyl and hydroxy reaction with the catalysis of EDC and HOBT. The ester linkage non-pH sensitive adamantane-PEG (AD-O-PEG) and the benzoic imine-containing pH sensitive adamantane-PEG (AD-B-PEG) conjugates were synthesized

as illustrated in Supporting Information Scheme S1. The non-pH sensitive AD-O-PEG was synthesized through the ester linkage in the presence of DCC and DMAP, and the structure was confirmed by ^{1}H NMR in $CDCl_3$. As shown in Supporting Information Fig. S1A, the newly formed characteristic signal at 4.2 ppm could be ascribed to the methylene next to the ester bond suggesting that ADA has been conjugated to PEG by an ester linkage. As for synthesis of AD-B-PEG, the mPEG was first modified by 4-carboxybenzaldehyde, and the adamantane-1-carboxylic acid was modified by ethanolamine. Then the benzoic-imine linkage formed between aldehyde group of benzene ring and amine of ethanolamine modified adamantane-1-carboxylic acid, which is more stable than the imine bond formed from aliphatic amine due to the π-π conjugation between benzene ring and imine. In Supporting Information Fig. S1B, the typical proton singlet attributed to the benzoic-imine (δ 8.33) indicated that AD-B-PEG was synthesized successfully.

3.2. *The pH-dependent hydrolysis of conjugates*

The fluorescamine method was performed to evaluate the pH-dependent hydrolysis of AD-B-PEG. Fluorescamine, an amine-reactive fluorescence derivative reagent, could react with primary amines specifically to produce high fluorescence, but its hydrolysis products and itself have no fluorescence. The fluorescence intensity of fluorescamine reaction indicated the PEG detachment level of AD-B-PEG at the different pH values since the primary amine was exposed after hydrolysis of benzoic imine. In Supporting Information Fig. S2, we could find out that AD-B-PEG was stable at pH 7.4, and less than 10% of the polymer was hydrolyzed up to 12 h, but it reached 58.75% at pH 6.5 and 73.95% at pH 5.0 only for 5 min. It indicated that the hydrolysis of benzoic imine was highly pH-dependent and very sensitive to the acidic environment. This result was similar to the previous studies that the hydrolysis reaction of benzoic imine was rapid under acidic condition[46,47].

The stability of the benzoic imine bond of HCBP in D_2O at different pH values was monitored by ^{1}H NMR to investigate whether HA-CD/AD-B-PEG inclusion complex (HCBP) possesses the same pH-sensitive hydrolysis effect or not. For prepared inclusion complex HCBP, the correlative characteristic peaks of HA-CD could be found except for the characteristic signals of AD-B-PEG (Supporting Information Fig. S3). And the peak signals of HA glycoside were partly overlapped with PEG methylene at chemical shift 3–4 ppm. In Supporting Information Fig. S3, there was no aldehyde proton peak observed at pH 7.4, but the clear aldehyde peak appeared around

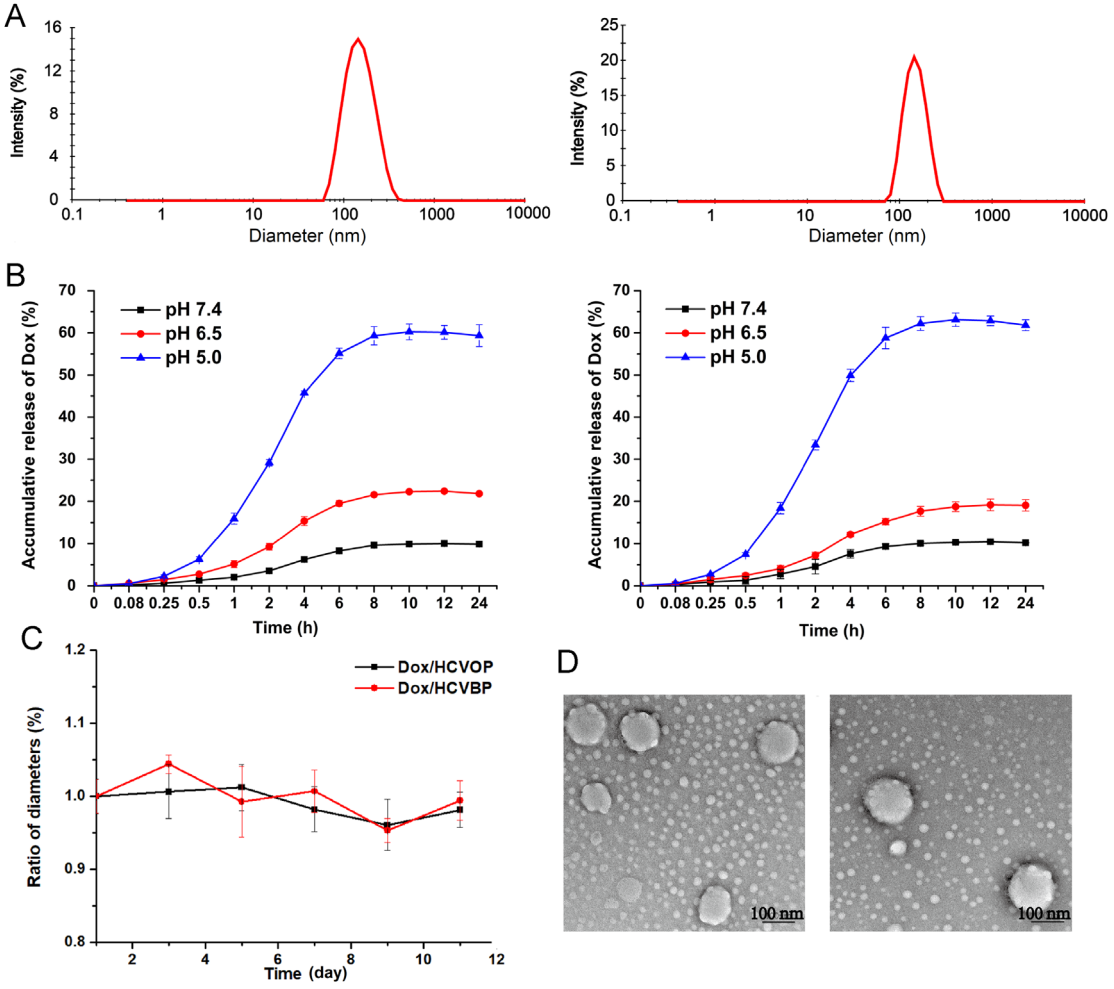

Figure 2 Physiochemical and pharmaceutical characteristics of Dox/HCVPs: (A) Size distribution by intensity of Dox/HCVOP (left) and Dox/HCVBP (right); (B) *In vitro* drug release behaviors of Dox/HCVOP (left) and Dox/HCVBP (right) in PBS (pH 7.4, 6.5 and 5.0); (C) Colloidal stability of Dox/HCVPs stored at 4 °C (D) Morphology observation of Dox/HCVOP (left) and Dox/HCVBP (right) by transmission electron microscope (data are mean ± SD, $n = 3$).

10 ppm when pH at 6.5 and 5.0. It suggested that PEG in HCBP inclusion complex also could be detached at tumor pHe.

3.3. *Preparation and characterization of Dox/HCVPs nanoparticles*

Dox/HCVPs were prepared according to our previously reported method. The lyophobic molecular VES as a bridge molecular could be inserted into the CD cavity *via* host–guest inclusion interaction to form a hydrophobic core for loading Dox and enhancing NPs stability. The hydrophilic hyaluronan and modified PEG shell would surround the hydrophobic core, finally a core-shell nanostructure (Fig. 1). The physiochemical and pharmaceutical characteristics of Dox/HCVPs were summarized in Supporting Information Table S1. Dox/HCVPs had negatively charged surfaces, spherical shape morphologies, about 140 nm average diameters, a uniform size distribution and high EE% for Dox (Fig. 2A and D). It was worth mentioning that there were some smaller particles around the nanoparticles. It could be the crystal of HEPES buffer salt formed during the sample preparation (Supporting Information Fig. S4). In Fig. 2C, Dox/HCVPs showed slight changes in particle size for ten days stored at 4 °C, suggesting the excellent colloidal stability. The release behavior of Dox from Dox/HCVPs at 37 °C for 24 h under different pH conditions was shown in Fig. 2B. They had similar release profiles due to the same architecture of hydrophobic core. A pH-responsive Dox release profiles could be observed, and it would be beneficial for their stable blood circulation without leakage and rapid release within tumor cells.

3.4. *CD44 receptor expression analysis*

CD44 is a transmembrane glycoprotein overexpressed on the surface of a variety of cancer cells and the most primary receptor of HA. It has been reported that CD44 density has a great effect on targeting efficiency[56]. Therefore, the expression of the CD44 receptor was analyzed by CLSM. As shown in Supporting Information Fig. S5, the apparent fluorescence intensity could be observed on the cell membranes of Hela, H460 and 4T1 cells, which indicated they were CD44-overexpressed cells. And high fluorescence signals were also found in frozen section of 4T1 tumor tissue excised from 4T1 tumor-bearing mice. Therefore, Hela and H460 cells were chosen as $CD44^{+}$ cells, and 4T1 tumor-bearing mice were used as tumor xenograft model for further studies.

3.5. *In vitro cytotoxicity effect and cellular uptake of Dox/HCVPs*

It should be considered that the incubation time of *in vitro* cytotoxicity procedure was as long as 48 h. Besides, the pH change of cell culture medium might affect cell growth and Dox/HCVPs had very different release behavior at pH 7.4 and 6.5 conditions. And the hydrolysis reaction of benzoic imine was rapid enough to detach the PEG within 30 min. Therefore, the Dox/HCVPs were pre-incubated under pH 6.5 condition for 30 min at 37 °C allowed to detach the PEG shell before use. Fig. 3A illustrated the cytotoxicity of free Dox and Dox/HCVPs at different concentrations on Hela and H460 cells measured using MTT assay, and the corresponding IC_{50} values were shown in Supporting Information Table S2. Compared with Dox/HCVOP, Dox/HCVBP showed a significantly higher cytotoxic effect on both Hela and H460 cells, even better than free Dox on H460 cells.

The corresponding cellular uptake of Dox/HCVPs was also studied by flow cytometry, and the result was shown in Fig. 3B. From the histogram of fluorescence intensity, the cellular uptake of NPs was time-dependent. Dox/HCVBP exhibited higher cellular uptake at each time-point on both cell types in comparison with Dox/HCVOP, and the differences were more remarkable at 3 h.

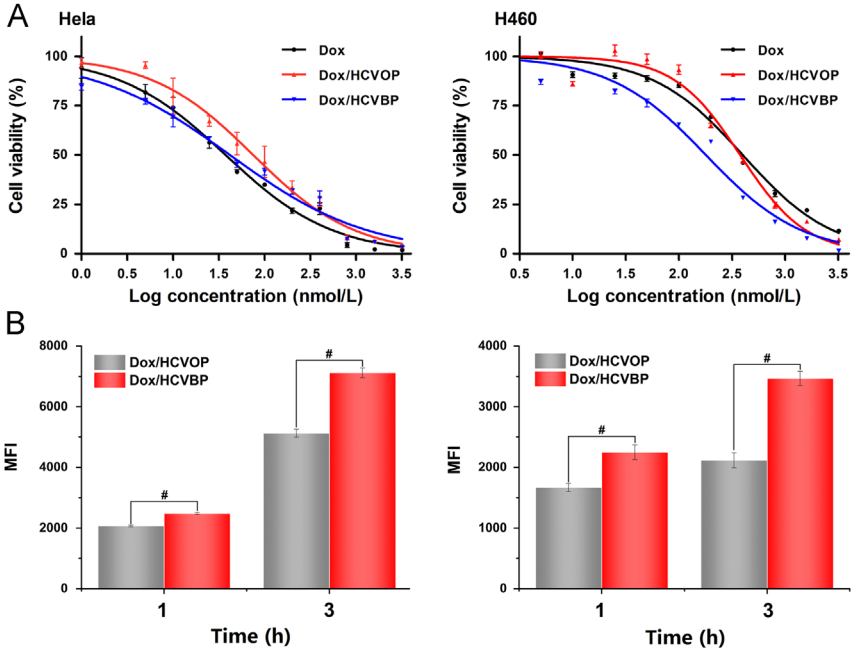

Figure 3 (A) Cell viabilities when treated with various formulations at different concentrations for 48 h on Hela (left) and H460 (right) cells. (B) Cellular uptake of Dox/HCVPs on Hela (left) and H460 (right) cells at 37 °C for 1 h and 3 h measured by flow cytometry (data are mean ± SD, $n=3$, $^{*}P<0.05$; $P<0.01$).

This tendency was similar to the result of *in vitro* cytotoxicity. It indicated that Dox/HCVBP enhanced *in vitro* cytotoxicity by increasing cellular uptake of NPs since PEG detachment under pH 6.5 condition.

3.6. *Mechanism of Dox/HCVPs cellular uptake*

The cellular uptake of Dox/HCVPs pretreated under pH 7.4 and 6.5 conditions was measured on Hela cells with or without free HA added for 3 h at 37 °C by flow cytometry, and the result was shown in Fig. 4. Firstly, the cellular uptake of Dox/HCVPs pretreated under pH 7.4 and 6.5 conditions for 30 min at 37 °C was measured to reveal the effect of pH on cellular uptake. As shown in Fig. 4B, the cellular uptake of Dox/HCOVP and Dox/HCVBP was similar at pH 7.4, but Dox/HCVBP showed much higher cellular uptake than Dox/HCVOP at pH 6.5. It indicated that pH had a great influence on cellular uptake of Dox/HCVBP but had little effect on Dox/HCVOP uptake. It might be attributed to the exposed HA ligands of Dox/HCVBP after detaching PEG shell at pH 6.5 which could make NPs transform from "stealth" state to "recognition" state.

To further disclose the role of HA in cellular internalization, the cellular uptake was investigated on Hela cells with or without pre-incubated with excessive free HA. In Fig. 4C, the cellular uptake of Dox/HCVPs was remarkably suppressed by added free HA, indicating the CD44 receptor-mediated cellular endocytosis. Around 25% fewer Dox/HCVOP uptakes observed at both pH 7.4 and 6.5 conditions, and there was no significant difference between them. On the contrary, the uptake of Dox/HCVBP declined by near 50% at pH 6.5, 2-fold greater than that at pH 7.4. This different inhibition effect of HA towards Dox/HCVBP at pH 7.4 and 6.5 further verified that Dox/HCVBP could increase the cellular uptake by converting to "recognition" state to improve the HA-CD44 recognition at pH 6.5.

3.7. *Intracellular trafficking of Dox/HCVPs by CLSM*

The intracellular trafficking of Dox/HCVPs was observed using CLSM to investigate their endosomal escape capability which is significant to antitumor drugs acting with DNA in the nucleus. For visualizing the subcellular localization, fluorescent dye LysoGreen was used to label acidic endo/lysosomes and DAPI for the cellular nucleus. As shown in Fig. 5, nearly all the red fluorescent of Dox was localized in endo/lysosomes when treated for 1 h, and a portion of Dox could be found in the cellular nucleus after 3 h incubation on both Dox/HCVPs NPs. And much stronger red fluorescent was shown on the cells treated with Dox/HCVBP than those incubated with Dox/HCVOP due to its higher cellular uptake at 3 h. It was so exciting that much red fluorescence was localized in the nucleus, but little was localized in endo/lysosomes on

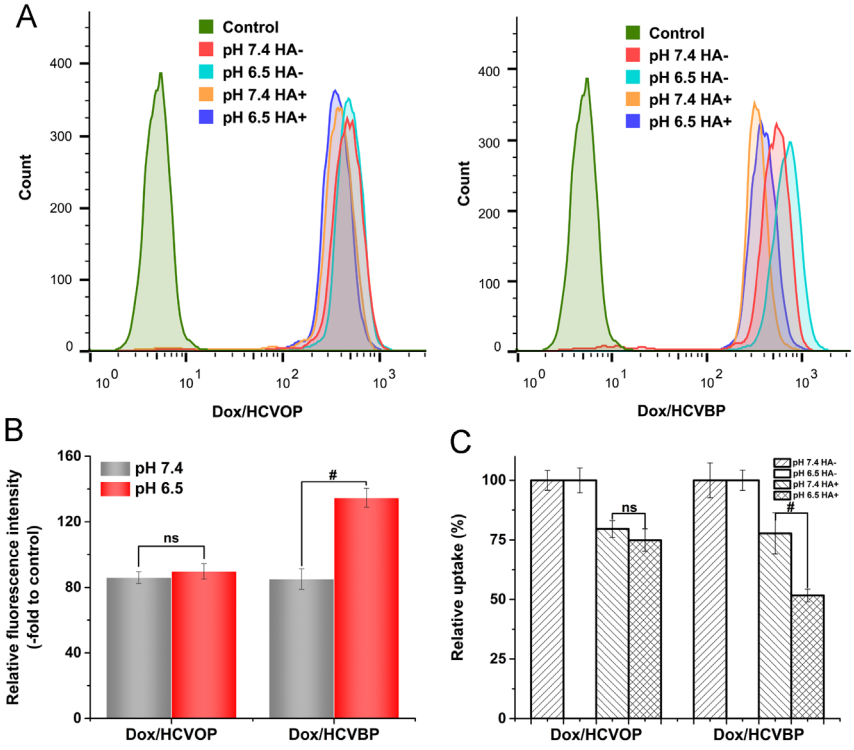

Figure 4 The cellular uptake mechanism investigations of Dox/HCVPs. (A) The cellular uptake histograms of Dox/HCOP (left) and Dox/HCVBP (right) pretreated under pH 7.4 and 6.5 conditions on Hela cells with or without free HA addition for 3 h at 37 °C was measured by flow cytometry. Groups are untreated (control), pH 7.4 without HA added (pH 7.4 HA-), pH 6.5 without HA added (pH 6.5 HA-), pH 7.4 with HA added (pH 7.4 HA+) and pH 6.5 with HA added (pH 6.5 HA+) respectively. (B) The cellular uptake of Dox/HCVPs pretreated under pH 7.4 and 6.5 conditions was quantified *via* fluorescent intensity relative to untreated controls. (C) The fluorescent intensity of Dox/HCVPs cellular uptake on free HA-treated Hela cells was normalized by the fluorescent intensity of cellular uptake on without free HA-treated Hela cells (data are mean ± SD, $n = 3$, $^{*}P < 0.05$; $P < 0.01$).

Dox/HCVBP group at 5 h. By contrast, a significant portion of fluorescence can still be observed in endo/lysosomes on Dox/HCVOP group. The corresponding colocalization coefficient PCC measured by Image pro plus 6.0 software further manifested this difference (Supporting Information Fig. S6), demonstrating that pH-triggered detached PEG shell is advantageous to the endosomal escape of NPs comparing with non-detached PEG-modified NPs.

3.8. *In vivo pharmacokinetic and biodistribution of Dox/HCVPs*

The *in vivo* pharmacokinetic of Dox solution, Dox/HCVOP and Dox/HCVBP were investigated in SD rats. The mean plasma concentration–time curves were shown in Fig. 6A and the main pharmacokinetic parameters were listed in Supporting Information Table S3. The two Dox/HCVPs showed the similar *in vivo* pharmacokinetic profiles. Although the AUC of Dox/HCVBP was a little less than Dox/HCVOP ($AUC_{0\text{-}t}$ were 3931.593 ± 770.229 and $4462.387 \pm 1001.992\ \mu g/L \cdot h$ respectively), they all significantly increased the AUC (about 4-fold) and remarkably prolonged the $t_{1/2}$ (about 3-fold) in comparison with Dox solution.

The biodistribution of DiR-loaded HCVPs NPs was carried out in 4T1 tumor-bearing mice by *ex vivo* imaging of major organs and tumor tissue. As shown in Fig. 6B, a strong fluorescence intensity could be found in the tumor of DiR-loaded HCVPs groups at 4 h post-administration, and it further increased at 24 h. However, bare fluorescence signals could be observed in tumor tissue of mice treated with free DiR and signal in other organs was much weaker. The enhanced accumulation of NPs in tumor should be attributed to the long circulation time in blood and the enhanced permeability and retention (EPR) effects in tumor of DiR/HCVPs. The corresponding quantitative analysis of the average fluorescence intensity of DiR in tumor tissues indicated that tumor accumulation did not have a significant difference between Dox/HCVOP and Dox/HCVBP (Supporting Information Fig. S7). These results further demonstrated that benzoic imine was stable enough in blood circulation for guaranteeing the "stealth" state of Dox/HCBP to prolong circulation time of NPs and enhance accumulation of tumors after intravenous injection. The strong fluorescence signals in liver, spleen, and lung even at 24 h might result from the metabolism characteristic of DiR.

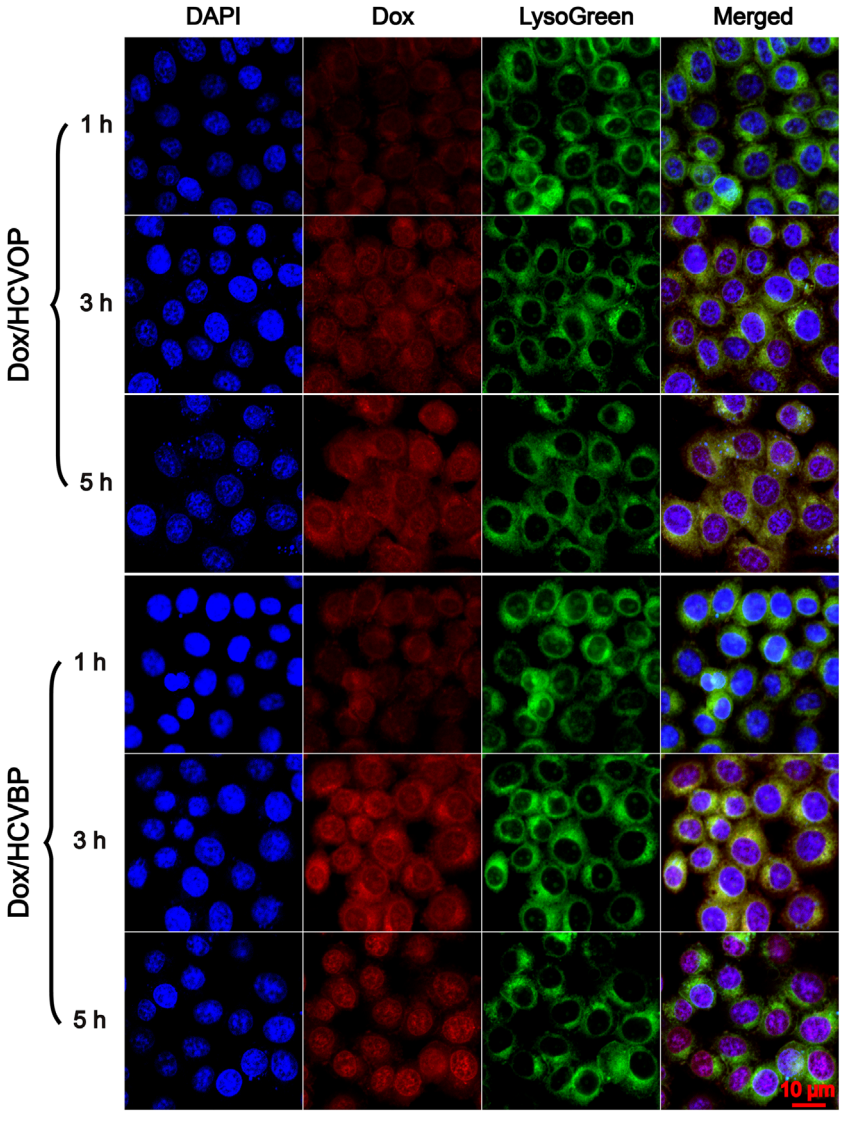

Figure 5 The intracellular trafficking of Dox/HCVPs was observed by confocal laser scanning microscope when incubated with Hela cells for 1, 3 and 5 h.

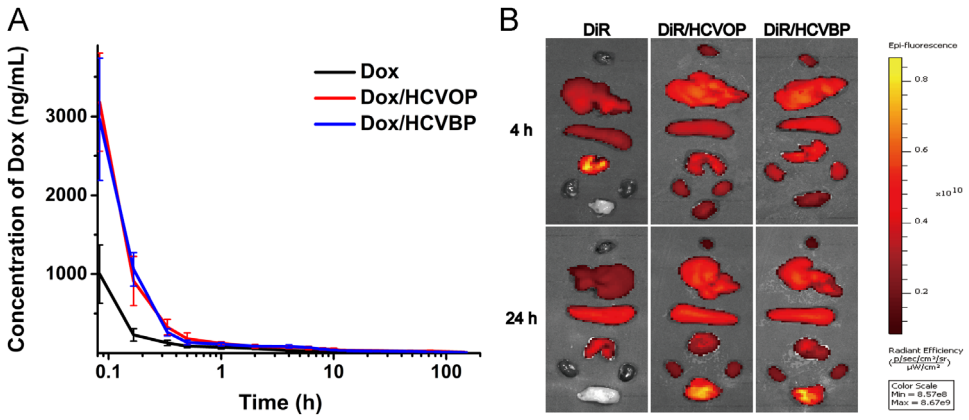

Figure 6 (A) Pharmacokinetic profiles of Dox, Dox/HCVOP and Dox/HCVBP in rats after a single intravenous administration of 5 mg/kg (data are mean ± SD, $n = 5$). (B) *Ex vivo* imaging of major organs and tumor tissue excised at 4 and 24 h post-administration of free DiR and DIR/HCVPs (from top to bottom: heart, liver, spleen, lung, kidney, and tumor).

3.9. *In vivo antitumor efficacy of Dox/HCVPs*

In vivo anticancer effect of Dox/HCVPs was studied in the 4T1 tumor xenograft model and the results were shown in Fig. 7. Tumors in the control group grew very fast and the average volume of tumor up to approximately 1000 mm^3 at the end of the investigation (Fig. 7A and B). In contrast, all of drug treatment groups exhibited antitumor efficacy to different degrees (Fig. 7A–C). Comparing with free Dox group, the significant inhibition effect of Dox/HCVPs on tumor growth might result from the different pharmacokinetic behavior that PEGylated Dox/HCVPs had longer circulation time than Dox solution. The high inhibition efficiency of Dox/HCVBP compared to Dox/HCVOP should be ascribed to the enhanced cellular uptake due to the transformation of "recognition" state and improved endosomal escapement after PEG shell detachment at tumor microenvironment. Notably, it was worth noting that free Dox solution caused a remarkable loss of body weight, indicating the severe systemic toxicity.

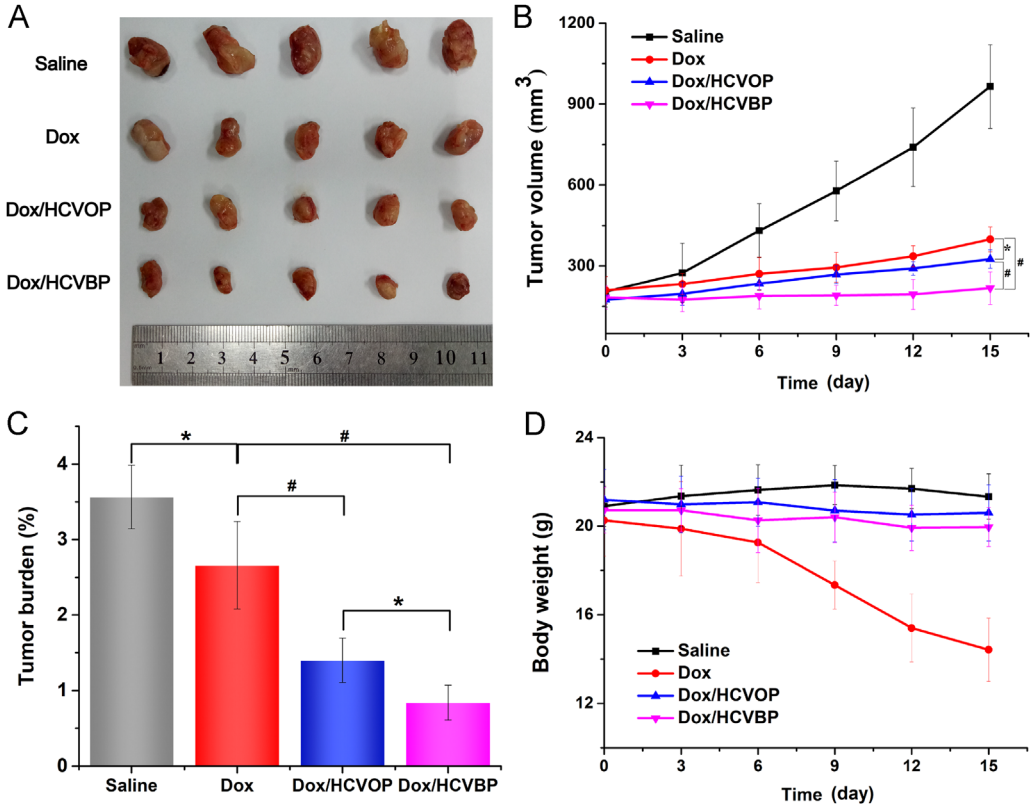

Figure 7 *In vivo* antitumor efficacy of Dox/HCVPs in 4T1 tumor-bearing mice. (A) Pictures of excised tumors in different groups at the end of the experiment. (B) 4T1 tumor growth curves of various groups with different treatments. (C) Tumor burden of various treatment groups was calculated by body weights and tumor weights at the end of the study. (D) The variation curves of 4T1 tumor-bearing mice body weight during the test (data are mean ± SD, $n = 5$, $^{*}P < 0.05$; $P < 0.01$).

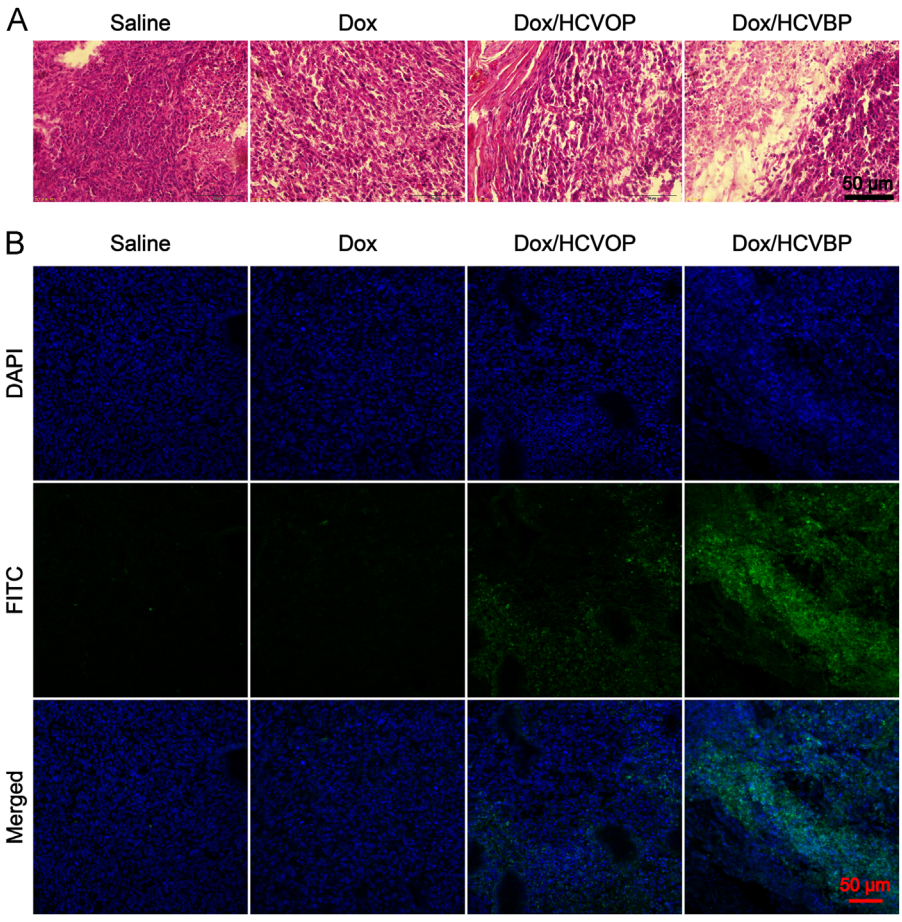

Figure 8 (A) Representative H &E staining of tumors in various groups. (B) TUNEL assay representative images of tumors after different treatments visualized using confocal laser scanning microscope.

Therefore, the tumor burden of Dox-treated groups was still high, although it showed an excellent antitumor effect. In contrast, Dox/HCVPs had little influence on body weight owing to their improved biodistribution and decreased systemic toxicity.

The tumor growth inhibition was further confirmed by H&E staining and TUNEL assay. As shown in Fig. 8A, an obvious blue-pink interlaced image could be observed in the tumor administrated with saline, indicating the active cell division and growth. And these tumor cells showed an infiltrative growth manner. By contrast, there were some vacuoles found in tumors of other groups, and Dox/HCVBP-treated tumor had more vacuoles, suggesting more apoptosis or necrosis of tumor cells. Additionally, TUNEL assay illustrated the obviously highest apoptosis level in tumor tissue of Dox/HCVBP group (Fig. 8B).

4. Conclusions

Dox-loaded HA-based transformable supramolecular nanoplatform was successfully prepared by introducing the pH_e-sensitive benzoic-imine-linked PEG for simultaneously prolonging blood circulation time and promoting active targeting cellular uptake of tumor cells. The *in vitro* and *in vivo* experiments strongly suggested that Dox/HCVBP significantly prolonged the circulation time, enhanced tumor cellular uptake, as well as endosomal escapement, and manifested the most effective antitumor effect on 4T1-bearing mice. In general, after intravenous injection, nanotransformable Dox/HCVBP could maximize the advantage of PEGylation to make NPs "stealth" for avoiding the unfavorable biodistribution and prolonging the blood circulation time. On the other hand, it could be converted into "recognition" state for enhancing cellular uptake and facilitating intracellular drug delivery by detaching the PEG shell at tumor microenvironment pH_e. Our findings paved the way to rationally design the natural ligand-targeting NPs by balancing two conflicting processes of tumor cellular uptake and *in vivo* nonspecific biodistribution.

Acknowledgments

This work was supported by the National Basic Research Program of China (No. 81573371) and the Key Projects of Liaoning Province Department of Education (No. 2017LZD03, China).

Appendix A. Supporting information

Supplementary data associated with this article can be found in the online version at https://doi.org/10.1016/j.apsb.2018.11.006.

References

1. Dosio F, Arpicco S, Stella B, Fattal E. Hyaluronic acid for anticancer drug and nucleic acid delivery. *Adv Drug Deliv Rev* 2016;**97**:204–36.

2. Jiang BP, Zhang L, Guo XL, Shen XC, Wang Y, Zhu Y, et al. Poly (*N*-phenylglycine)-based nanoparticles as highly effective and targeted near-infrared photothermal therapy/photodynamic therapeutic agents for malignant melanoma. *Small* 2017;**13**:1602496.
3. Zhou Y, Quan G, Wu Q, Zhang X, Niu B, Wu B, et al. Mesoporous silica nanoparticles for drug and gene delivery. *Acta Pharm Sin B* 2018;**8**:165–77.
4. Platt VM, Szoka Jr. FC. Anticancer therapeutics: targeting macromolecules and nanocarriers to hyaluronan or CD44, a hyaluronan receptor. *Mol Pharm* 2008;**5**:474–86.
5. Choi KY, Chung H, Min KH, Yoon HY, Kim K, Park JH, et al. Self-assembled hyaluronic acid nanoparticles for active tumor targeting. *Biomaterials* 2010;**31**:106–14.
6. Wang M, Li J, Li X, Mu H, Zhang X, Shi Y, et al. Magnetically and pH dual responsive dendrosomes for tumor accumulation enhanced folate-targeted hybrid drug delivery. *J Control Release* 2016;**232**:161–74.
7. Battogtokh G, Ko YT. Graphene oxide-incorporated pH-responsive folate-albumin-photosensitizer nanocomplex as image-guided dual therapeutics. *J Control Release* 2016;**234**:10–20.
8. Leamon CP, Low PS. Folate-mediated targeting: from diagnostics to drug and gene delivery. *Drug Discov Today* 2001;**6**:44–51.
9. Daniels TR, Bernabeu E, Rodríguez JA, Patel S, Kozman M, Chiappetta DA, et al. The transferrin receptor and the targeted delivery of therapeutic agents against cancer. *BBA-Gen Subj* 2012;**1820**:291–317.
10. Han X, Li Z, Sun J, Luo C, Li L, Liu Y, et al. Stealth CD44-targeted hyaluronic acid supramolecular nanoassemblies for doxorubicin delivery: probing the effect of uncovalent pegylation degree on cellular uptake and blood long circulation. *J Control Release* 2015;**197**:29–40.
11. Chi Y, Yin X, Sun K, Feng S, Liu J, Chen D, et al. Redox-sensitive and hyaluronic acid functionalized liposomes for cytoplasmic drug delivery to osteosarcoma in animal models. *J Control Release* 2017;**261**:113–25.
12. Choi KY, Min KH, Yoon HY, Kim K, Park JH, Kwon IC, et al. PEGylation of hyaluronic acid nanoparticles improves tumor targetability *in vivo*. *Biomaterials* 2011;**32**:1880–9.
13. Ran R, Liu Y, Gao H, Kuang Q, Zhang Q, Tang J, et al. Enhanced gene delivery efficiency of cationic liposomes coated with PEGylated hyaluronic acid for anti P-glycoprotein siRNA: a potential candidate for overcoming multi-drug resistance. *Int J Pharm* 2014;**477**:590–600.
14. Yoon HY, Koo H, Choi KY, Lee SJ, Kim K, Kwon IC, et al. Tumor-targeting hyaluronic acid nanoparticles for photodynamic imaging and therapy. *Biomaterials* 2012;**33**:3980–9.
15. Qhattal HS, Hye T, Alali A, Liu X. Hyaluronan polymer length, grafting density, and surface poly(ethylene glycol) coating influence *in vivo* circulation and tumor targeting of hyaluronan-grafted liposomes. *ACS Nano* 2014;**8**:5423–40.
16. Ju Y, Cui J, Sun H, Müllner M, Dai Y, Guo J, et al. Engineered metal-phenolic capsules show tunable targeted delivery to cancer cells. *Biomacromolecules* 2016;**17**:2268–76.
17. Mishra P, Nayak B, Dey RK. PEGylation in anti-cancer therapy: an overview. *Asian J Pharm Sci* 2016;**11**:337–48.
18. Tu Y, Zhu L. Enhancing cancer targeting and anticancer activity by a stimulus-sensitive multifunctional polymer–drug conjugate. *J Control Release* 2015;**212**:94–102.
19. Wang T, Wang D, Liu J, Feng B, Zhou F, Zhang H, et al. Acidity-triggered ligand-presenting nanoparticles to overcome sequential drug delivery barriers to tumors. *Nano Lett* 2017;**17**:5429–36.
20. Lv Y, Xu C, Zhao X, Lin C, Yang X, Xin X, et al. Nanoplatform assembled from a CD44-targeted prodrug and smart liposomes for dual targeting of tumor microenvironment and cancer cells. *ACS Nano* 2018;**12**:1519–36.
21. Liu Y, Wang W, Yang J, Zhou C, Sun J. pH-Sensitive polymeric micelles triggered drug release for extracellular and intracellular drug targeting delivery. *Asian J Pharm Sci* 2013;**8**:159–67.
22. Li R, He Y, Zhang S, Qin J, Wang J. Cell membrane-based nanoparticles: a new biomimetic platform for tumor diagnosis and treatment. *Acta Pharm Sin B* 2018;**8**:14–22.
23. Li HJ, Du JZ, Liu J, Du XJ, Shen S, Zhu YH, et al. Smart superstructures with ultrahigh pH-sensitivity for targeting acidic tumor microenvironment: instantaneous size switching and improved tumor penetration. *ACS Nano* 2016;**10**:6753–61.
24. Zhang M, Liu J, Kuang Y, Li Q, Chen H, Ye H, et al. "Stealthy" chitosan/mesoporous silica nanoparticle based complex system for tumor-triggered intracellular drug release. *J Mater Chem B* 2016;**4**:3387–97.
25. Zeng X, Liu G, Tao W, Ma Y, Zhang X, He F, et al. A drug-self-gated mesoporous antitumor nanoplatform based on pH-sensitive dynamic covalent bond. *Adv Funct Mater* 2017;**27**:1605985.
26. Zhao C, Deng H, Xu J, Li S, Zhong L, Shao L, et al. "Sheddable" PEG-lipid to balance the contradiction of PEGylation between long circulation and poor uptake. *Nanoscale* 2016;**8**:10832–42.
27. Yang Y, Xu L, Zhu W, Feng L, Liu J, Chen Q, et al. One-pot synthesis of pH-responsive charge-switchable PEGylated nanoscale coordination polymers for improved cancer therapy. *Biomaterials* 2018;**156**:121–33.
28. Chen X, Liu L, Jiang C. Charge-reversal nanoparticles: novel targeted drug delivery carriers. *Acta Pharm Sin B* 2016;**6**:261–7.
29. Zhang W, Cheng Q, Guo S, Lin D, Huang P, Liu J, et al. Gene transfection efficacy and biocompatibility of polycation/DNA complexes coated with enzyme degradable PEGylated hyaluronic acid. *Biomaterials* 2013;**34**:6495–503.
30. Shin JM, Oh SJ, Kwon S, Deepagan VG, Lee M, Song SH, et al. A PEGylated hyaluronic acid conjugate for targeted cancer immunotherapy. *J Control Release* 2017;**267**:181–90.
31. Li D, Ma Y, Du J, Tao W, Du X, Yang X, et al. Tumor acidity/NIR controlled interaction of transformable nanoparticle with biological systems for cancer therapy. *Nano Lett* 2017;**17**:2871–8.
32. Zhu L, Wang T, Perche F, Taigind A, Torchilin VP. Enhanced anticancer activity of nanopreparation containing an MMP2-sensitive PEG-drug conjugate and cell-penetrating moiety. *Proc Natl Acad Sci U S A* 2013;**110**:17047–52.
33. Romberg B, Hennink WE, Storm G. Sheddable coatings for long-circulating nanoparticles. *Pharm Res* 2008;**25**:55–71.
34. Fay F, Hansen L, Hectors SJ, Sanchez-Gaytan BL, Zhao Y, Tang J, et al. Investigating the cellular specificity in tumors of a surface-converting nanoparticle by multimodal imaging. *Bioconjug Chem* 2017;**28**:1413–21.
35. Yang XZ, Du JZ, Dou S, Mao CQ, Long HY, Wang J. Sheddable ternary nanoparticles for tumor acidity-targeted siRNA delivery. *ACS Nano* 2012;**6**:771–81.
36. Fan Y, Li C, Li F, Chen D. pH-activated size reduction of large compound nanoparticles for *in vivo* nucleus-targeted drug delivery. *Biomaterials* 2016;**85**:30–9.
37. Zhao J, Liu J, Xu S, Zhou J, Han S, Deng L, et al. Graft copolymer nanoparticles with pH and reduction dual-induced disassemblable property for enhanced intracellular curcumin release. *ACS Appl Mater Interfaces* 2013;**5**:13216–26.
38. Guan X, Guo Z, Wang T, Lin L, Chen J, Tian H, et al. A pH-responsive detachable PEG shielding strategy for gene delivery system in cancer therapy. *Biomacromolecules* 2017;**18**:1342–9.
39. Vander Heiden MG, Cantley LC, Thompson CB. Understanding the Warburg effect: the metabolic requirements of cell proliferation. *Science* 2009;**324**:1029–33.
40. Lyssiotis CA, Kimmelman AC. Metabolic interactions in the tumor microenvironment. *Trends Cell Biol* 2017;**27**:863–75.
41. Yamagata M, Hasuda K, Stamato T, Tannock IF. The contribution of lactic acid to acidification of tumours: studies of variant cells lacking lactate dehydrogenase. *Br J Cancer* 1998;**77**:1726–31.
42. Qiu L, Zhu M, Gong K, Peng H, Ge L, Zhao L, et al. pH-Triggered degradable polymeric micelles for targeted anti-tumor drug delivery. *Mat Sci Eng C: Mater Biol Appl* 2017;**78**:912–22.
43. Guo X, Wang L, Duval K, Fan J, Zhou S, Chen Z. Dimeric drug polymeric micelles with acid-active tumor targeting and FRET-traceable drug release. *Adv Mater* 2018;**30** Available from: ⟨https://doi.org/10.1002/adma.201705436⟩ .
44. Wei J, Shuai X, Wang R, He X, Li Y, Ding M, et al. Clickable and imageable multiblock polymer micelles with magnetically guided and

PEG-switched targeting and release property for precise tumor theranosis. *Biomaterials* 2017;**145**:138–53.
45. Zhang J, Zheng Y, Xie X, Wang L, Su Z, Wang Y, et al. Cleavable multifunctional targeting mixed micelles with sequential pH-triggered TAT peptide activation for improved antihepatocellular carcinoma efficacy. *Mol Pharm* 2017;**14**:3644–59.
46. Gu J, Cheng WP, Liu J, Lo SY, Smith D, Qu X, et al. pH-Triggered reversible "stealth" polycationic micelles. *Biomacromolecules* 2008;**9**:255–62.
47. Ding C, Gu J, Qu X, Yang Z. Preparation of multifunctional drug carrier for tumor-specific uptake and enhanced intracellular delivery through the conjugation of weak acid labile linker. *Bioconjug Chem* 2009;**20**:1163–70.
48. Yang Z, Sun N, Cheng R, Zhao C, Liu Z, Li X, et al. pH multistage responsive micellar system with charge-switch and PEG layer detachment for co-delivery of paclitaxel and curcumin to synergistically eliminate breast cancer stem cells. *Biomaterials* 2017;**147**:53–67.
49. Li Y, Song L, Lin J, Ma J, Pan Z, Zhang Y, et al. Programmed nanococktail based on pH-responsive function switch for self-synergistic tumor-targeting therapy. *ACS Appl Mater Interfaces* 2017;**9**:39127–42.
50. Zhao G, Long L, Zhang L, Peng M, Cui T, Wen X, et al. Smart pH-sensitive nanoassemblies with cleavable PEGylation for tumor targeted drug delivery. *Sci Rep* 2017;**7**:3383.
51. Cheng W, Liang C, Wang X, Tsai HI, Liu G, Peng Y, et al. A drug-self-gated and tumor microenvironment-responsive mesoporous silica vehicle: "four-in-one" versatile nanomedicine for targeted multidrug-resistant cancer therapy. *Nanoscale* 2017;**9**:17063–73.
52. Fitzgerald KA, Malhotra M, Gooding M, Sallas F, Evans JC, Darcy R, et al. A novel, anisamide-targeted cyclodextrin nanoformulation for siRNA delivery to prostate cancer cells expressing the sigma-1 receptor. *Int J Pharm* 2016;**499**:131–45.
53. Song X, Zhu JL, Wen Y, Zhao F, Zhang ZX, Li J. Thermoresponsive supramolecular micellar drug delivery system based on star-linear pseudo-block polymer consisting of β-cyclodextrin-poly(*N*-isopropylacrylamide) and adamantyl-poly(ethylene glycol). *J Colloid Interface Sci* 2017;**490**:372–9.
54. Song N, Ding M, Pan Z, Li J, Zhou L, Tan H, et al. Construction of targeting-clickable and tumor-cleavable polyurethane nanomicelles for multifunctional intracellular drug delivery. *Biomacromolecules* 2013;**14**:4407–19.
55. Mo R, Sun Q, Xue J, Li N, Li W, Zhang C, et al. Multistage pH-responsive liposomes for mitochondrial-targeted anticancer drug delivery. *Adv Mater* 2012;**24**:3659–65.
56. Qhattal HS, Liu X. Characterization of CD44-mediated cancer cell uptake and intracellular distribution of hyaluronan-grafted liposomes. *Mol Pharm* 2011;**8**:1233–46.